WILEY

RESEARCH ARTICLE

Regional and network properties of white matter function in Parkinson's disease

Gong-Jun Ji[1] | Cuiping Ren[2,3,4] | Ying Li[2,3,4] | Jinmei Sun[2,3,4] | Tingting Liu[2,3,4] |
Yaxiang Gao[3,4] | Dongzhang Xue[5] | Longshan Shen[6] | Wen Cheng[7] | Chunyan Zhu[1,3,4] |
Yanghua Tian[2,3,4] | Panpan Hu[2,3,4] | Xianwen Chen[2,3,4] | Kai Wang[2,3,4]

[1]Department of Medical Psychology, Chaohu Clinical Medical College, Anhui Medical University, Hefei, China

[2]Department of Neurology, The First Affiliated Hospital of Anhui Medical University, Hefei, China

[3]Collaborative Innovation Centre of Neuropsychiatric Disorder and Mental Health, Hefei, China

[4]Anhui Province Key Laboratory of Cognition and Neuropsychiatric Disorders, Hefei, China

[5]Department of Neurology, The 123 Hospital of People's Liberation Army, Bengbu, China

[6]Department of Imaging, The Second Affiliated Hospital of Bengbu Medical College, Bengbu, China

[7]College of Literature and Education, Bengbu College, Bengbu, China

Correspondence
Kai Wang and Xianwen Chen, Department of Neurology, The First Affiliated Hospital of Anhui Medical University, Hefei 230000, China.
Emails: wangkai1964@126.com; chxwmail@aliyun.com

Abstract

Parkinson's disease (PD) is a neurodegenerative disorder with dysfunction in cortices as well as white matter (WM) tracts. While the changes to WM structure have been extensively investigated in PD, the nature of the functional changes to WM remains unknown. In this study, the regional activity and functional connectivity of WM were compared between PD patients (n = 57) and matched healthy controls (n = 52), based on multimodel magnetic resonance imaging data sets. By tract-based spatial statistical analyses of regional activity, patients showed decreased structural-functional coupling in the left corticospinal tract compared to controls. This tract also displayed abnormally increased functional connectivity within the left post-central gyrus and left putamen in PD patients. At the network level, the WM functional network showed small-worldness in both controls and PD patients, yet it was abnormally increased in the latter group. Based on the features of the WM functional connectome, previously un-evaluated individuals could be classified with fair accuracy (73%) and area under the curve of the receiver operating characteristics (75%). These neuroimaging findings provide direct evidence for WM functional changes in PD, which is crucial to understand the functional role of fiber tracts in the pathology of neural circuits.

KEYWORDS

classification, functional connectivity, graph theory, magnetic resonance imaging, Parkinson's disease, tract-based spatial statistics, white matter

1 | INTRODUCTION

Parkinson's disease (PD) is the second most common neurodegenerative disease after Alzheimer's disease (Dorsey et al., 2007). Patients typically manifest with motor dysfunctions such as bradykinesia, rigidity, resting tremor, and postural instability. The underlying mechanism of PD is understood to be the loss of dopaminergic cells in the substantia nigra pars compacta. However, studies using animal models of PD have demonstrated that pathological changes were not restricted to the cell bodies (Burke & O'Malley, 2013); damage to the projecting axons of substantia nigral neurons can also be observed in early stages of PD (Tagliaferro et al., 2015). Thus, investigating the structural and functional changes to brain white matter (WM) is critical to understand the pathological mechanism of PD.

Diffusion tensor imaging (DTI) is a powerful tool to investigate microstructural alterations to the human brain in vivo. In PD, this technique has been combined with voxel- or region-of-interest (ROI)-wise (Atkinson-Clement, Pinto, Eusebio, & Coulon, 2017; Schwarz et al., 2013), and graph-theoretical analyses (Aarabi et al., 2015; Li et al., 2017; Nigro et al., 2016; Pereira et al., 2015). Tract-based spatial statistics (TBSS) is a voxel-wise method, specifically developed to minimize the methodological pitfalls caused by misalignment and misregistration in conventional voxel-based analyses (Smith et al., 2006). However, the TBSS findings in PD patients have differed between studies. While some studies have found normal fractional anisotropy (FA) in PD patients (Hattori et al., 2012; Worker et al., 2014), others reported limited (Galantucci et al., 2017) or widespread (Li, Ren, Cao, & Huang, 2017) abnormalities in brain WM. When using graph-theoretical analysis, structural topological properties of regions (i.e., small-worldness and efficiency) can be estimated by the diffusion features of fiber tracts (Gong et al., 2009; Hagmann et al., 2008). It has been demonstrated that the brain structural network is a small-world network with many local connections, and a few long-distance connections, an arrangement which is optimal for synchronizing neuronal activity between different brain regions (Bullmore & Sporns, 2009; Ji et al., 2015). This small-worldness has been shown to be disrupted in PD patients if they also present with mild cognitive impairment (Galantucci et al., 2017). All these advances have improved our understanding of the structural changes that underlie clinical symptoms of PD (Hall et al., 2016), and may also help in classifying healthy controls or patients with other neurodegeneration diseases (Cochrane & Ebmeier, 2013).

In contrast to the number of structural studies, considerably little functional imaging research has focused on brain WM. This is probably because the origin of the functional magnetic resonance imaging (fMRI) signal in WM was still largely unknown until recently (Gawryluk, Mazerolle, & D'Arcy, 2014), when studies indicated that functional activation in WM can be revealed by the blood oxygenation level dependent (BOLD) signal. For instance, different subregions of the corpus callosum can be exclusively activated by their functionally related tasks (Courtemanche, Sparrey, Song, MacKay, & D'Arcy, 2018; Fabri, Pierpaoli, Barbaresi, & Polonara, 2014; Fabri & Polonara, 2013; Fabri, Polonara, Mascioli, Salvolini, & Manzoni, 2011; Gawryluk, D'Arcy, Mazerolle, Brewer, & Beyea, 2011; Gawryluk, Mazerolle, Beyea, & D'Arcy, 2014; Haberling, Badzakova-Trajkov, & Corballis, 2011; Mazerolle et al., 2010; Mazerolle,

D'Arcy, & Beyea, 2008). During resting state (i.e., absence of task requirement on subject), the BOLD signal in WM exhibits a topological organization rather than random distribution as noise (Ji, Liao, Chen, Zhang, & Wang, 2017). As the fibers are tracked using DTI data, anatomical bundles are able to be identified by resting-state fMRI data as well (Ding et al., 2013; Marussich, Lu, Wen, & Liu, 2017; Peer, Nitzan, Bick, Levin, & Arzy, 2017). Additionally, the WM function, estimated by the low-frequency BOLD signal, can be modulated by different tasks (Ding et al., 2018; Ji, Liao, et al., 2017; Marussich et al., 2017; Wu et al., 2017). For instance, visual stimulation was found to exclusively increase the amplitude of low-frequency fluctuation (ALFF) of bilateral optic radiations (Ji, Liao, et al., 2017). All these evidences suggested that the BOLD signal can be used to estimate WM function, a novel perspective that has motivated some recent investigation in different brain disorders. In Alzheimer's disease, it has been found that the resting-state WM function was associated with regional glucose metabolism and correlated with memory function (Makedonov, Chen, Masellis, & MacIntosh, 2016). Combining dynamic functional connectivity in WM could provide valuable information in classifying mild cognitive impairment patients and healthy controls (Chen et al., 2017). More recently, Jiang and colleagues classified WM into several functional networks as a previous study (Peer et al., 2017), and estimated their disrupted synchronization with gray matter (GM) function in schizophrenia patients (Jiang et al., 2018).

In this study, we aimed to comprehensively reveal the resting-state function of WM in PD patients. To this end, both voxel and network level analyses were performed. As our previous work indicated that the ALFF was significantly correlated with FA in WM (Ji, Liao, et al., 2017), supporting the idea that structural-functional coupling is a basic organizing principle in healthy subjects (Honey et al., 2009; Wang, Dai, Gong, Zhou, & He, 2014), the ALFF/FA ratio would be adopted here as the regional level measure. At the network level, the topological properties of WM functional network would be investigated using graph-theoretical analysis.

2 | MATERIALS AND METHODS

2.1 | Subjects

A total of 57 patients diagnosed with PD at the First Affiliated Hospital of Anhui Medical University were consecutively enrolled in this study. The inclusion criteria were as follows: patients fulfilling the idiopathic PD diagnosis according to the UK brain bank criteria, age older than 45 years, Mini-Mental State Examination score higher than 24. Exclusion criteria were a history of addiction, psychiatric disorders, or neurologic diseases other than PD; focal brain lesions on T1-weighted and T2-weighted fluid-attenuated inversion recovery images; and head motion exceeding 3 mm in translation or 3° in rotation during fMRI scanning. Symptoms of 51 of the patients were assessed using the Unified Parkinson's Disease Rating Scale III (UPDRS-III) and the Hoehn-Yahr (H-Y) stage after medication withdrawal for at least 12 hr, the so-called off state. The other six patients were assessed in a medication-on state, without medication withdrawal. Cognitive functions were estimated using the Montreal cognitive assessment, a verbal fluency test, and digit span (forward and backward). Notably,

TABLE 1 Demographic and clinical features

	PD	HC	Statistics	p value
Sample size (M/F)	29/28	20/32	1.69	.19[a]
Age (years)	59.5 ± 1.21	60.6 ± 1.22	0.61	.54[b]
Education (years)	8.4 ± 0.66	9.3 ± 0.56	1.08	.28[b]
Duration (years)	4.6 ± 0.61	NA	NA	NA
UPDRS-III	25 ± 1.41 (n = 55)*	NA	NA	NA
H-Y	1.3 ± 0.35 (n = 50)*	NA	NA	NA
MMSE	28.1 ± 0.32	28.4 ± 0.21	0.90	.36[b]
MoCA	23.7 ± 0.73 (n = 54)*	25.5 ± 0.62 (n = 32)*	1.70	.10[b]
VFT	16.5 ± 0.62 (n = 51)*	17.9 ± 0.57 (n = 49)*	1.67	.10[b]
DST (forward)	7.2 ± 0.23 (n = 49)*	6.9 ± 0.21 (n = 48)*	0.87	.39[b]
DST (backward)	4.4 ± 0.37 (n = 49)*	4.7 ± 0.23 (n = 48)*	0.68	.50[b]

Data are mean ± SE. [a]Chi-square test; [b]two-sample t test.
Abbreviations: DST = Digit Span Test; F = Female; HC = Healthy Control; M = Male; MoCA = Montreal Cognitive Assessment; NA = Not Available; PD = Parkinson's Disease; UPDRS = Unified Parkinson's Disease Rating Scale; VFT = Verbal Fluency Test; H-Y = Hoehn and Yahr stage.
*Data in parentheses indicates the number of subjects in each test. Data without an asterisk is computed on all subjects.

some subjects did not complete all tests (Table 1). Healthy controls consisted of 52 age, sex, and education-matched individuals consecutively enrolled from the local community. These participants had no history of neurological disorders or psychiatric illnesses, and no gross abnormalities in their brain MRI. This study protocol was reviewed and approved by the Medical Ethics Committee of Anhui Medical University. Written informed consent was obtained from all participants.

## 2.2 | Multimodel MRI data acquisition

Functional, structural, and diffusion MRI data sets were obtained at University of Science and Technology of China with a 3-T scanner (Discovery 750; GE Healthcare, Milwaukee, WI). Foam padding was used to minimize head motion for all subjects. Participants were instructed to rest with their eyes closed without falling asleep during resting-state fMRI scanning. Functional images (217 volumes) were acquired using a single shot gradient-recalled echo planar imaging sequence (repetition/echo time, 2,400/30 ms; flip angle, 90°). Images of 46 transverse sections (field of view, 192 × 192 mm^2; 64 × 64 in-plane matrix; section thickness without intersection gap, 3 mm; voxel size, 3 × 3 × 3 mm^3) were acquired parallel to the anteroposterior commissure line. Subsequently, high-spatial-resolution T1-weighted anatomic images were acquired in the sagittal orientation using a three-dimensional brain-volume sequence (repetition/echo time, 8.16/3.18 ms; flip angle, 12°; field of view, 256 × 256 mm^2; 256 × 256 matrix; section thickness, 1 mm, without intersection gap; voxel size, 1 × 1 × 1 mm^3; 188 sections). Finally, a spin-echo echo planar imaging sequence was used to produce 64 volumes with diffusion gradients applied along 64 noncollinear directions (b = 1,000 s/mm^2) and five volumes without diffusion weighting (b = 0 s/mm^2). Each volume consisted of 69 contiguous axial sections (TR = 6,900 ms, TE = minimum flip angle = 90°, field of view = 256 × 256 mm^2, matrix = 128 × 128, slice thickness = 2 mm, no interslice gap).

2.3 | Functional data processing

Functional images were preprocessed using the Data Processing Assistant for Resting-State fMRI (http://rfmri.org/DPARSF) (Yan & Zang, 2010), TMStarget (Ji, Yu, Liao, & Wang, 2017), and SPM12 (http://www.fil.ion.ucl.ac.uk/spm/software/spm12) (Figure 1). We deleted the first five functional volumes, and then performed slice timing and realignment for the rest of the images. Structural images were then coregistered with these preprocessed functional images, and segmented into GM, WM, and cerebrospinal fluid (CSF) by Diffeomorphic Anatomical Registrations through Exponentiated Lie Algebra (DARTEL) (Ashburner, 2007). Based on the transformation matrix produced by DARTEL, a CSF mask in Montreal Neurological Institute (MNI) space (70% threshold on SPM12's a priori probability map) was transformed into individual functional space. The mean signal in the CSF mask and the 24 head motion parameters (Friston, Williams, Howard, Frackowiak, & Turner, 1996) were regressed out from the functional images in each subject's individual space. To avoid elimination of signals of interest, we did not include WM and global brain signal as nuisance regressors (Ji, Liao, et al., 2017; Peer et al., 2017).

To avoid mixing signals between GM and WM, subsequent processing for the functional images was performed for GM and WM separately (Figure 1). First, individual masks were produced using a 50% and 90% threshold on the probability map of GM and WM (produced by structural segmentation), respectively. To correctly classify deep brain structures that were assigned as WM in DARTEL, the (25% probability) Harvard-Oxford Atlas (Desikan et al., 2006) was transformed into an individual's functional space (using the inverse matrix during structural segmentation) to remove subcortical nuclei (i.e., bilateral caudate, pallidum, putamen, accumbens, thalamus, and brainstem) from the WM mask. Second, functional images were spatially separated into GM and WM images based on these two masks. Third, the GM images were normalized into MNI space by structural segmentation, smoothed (6 mm full-width half-maximum, isotropic), and filtered (0.01–0.1 Hz) for computing functional connectivity and ALFF. The functional connectivity was transformed to Fisher's z value, while the ALFF was standardized by zero-mean normalization. Fourth, two different processes were performed for the WM images. One was the same as GM, which was performed for further connectivity and network analysis. The other was computing ALFF map and transforming it into diffusion space using
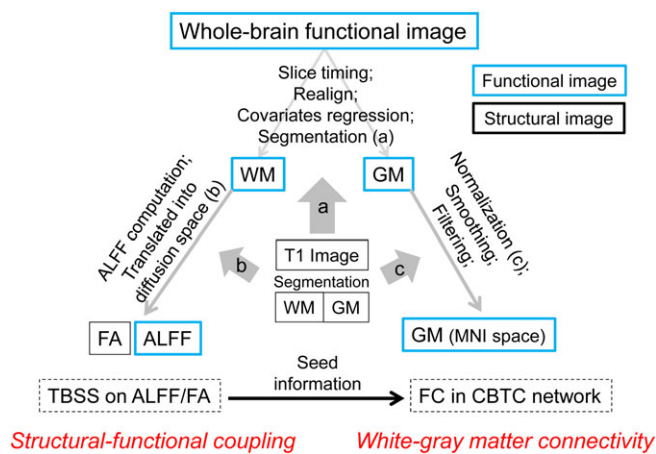
FIGURE 1 Flow chart of regional-level data processing. Resting-state functional images were segmented into white matter (WM) and gray matter (GM) via the segmentation information of structural images. The amplitude of low-frequency fluctuation (ALFF) maps in WM was transformed into diffusion space by the coregistration information between structural and fractional anisotropy (FA) images. Statistical findings on the ALFF/FA ratio between patient and control groups provided seed information for the WM-GM functional connectivity analysis in Montreal neurological institute (MNI) space. Abbreviations: CBTC = corticobasal ganglia-thalamocortical; FC = functional connectivity [Color figure can be viewed at wileyonlinelibrary.com]

structure-FA coregistration, which was performed for structural-functional coupling analysis (see section 2.4).

2.4 | Diffusion data processing

Diffusion images were preprocessed and analyzed using fMRIB's Software Library (FSL) (http://fsl.fmrib.ox.ac.uk/fsl). For each subject, head motion and eddy current-induced distortion were corrected by *eddy* function. Then, FA maps were calculated by fitting the diffusion tensor model at each voxel. TBSS analysis was first performed for FA images using the routine steps (https://fsl.fmrib.ox.ac.uk/fsl/fslwiki/TBSS) (Smith et al., 2006). Specifically, FA images were transformed into MNI space by nonlinear registration. Then, a mean skeletonized FA image was created by thinning the FA images, and thresholded by FA > 0.20 to include the major WM pathways, but exclude peripheral tracts and GM. Finally, each subject's FA image was projected onto the skeleton by filling the skeleton with FA values from the nearest relevant tract center.

To analyze the WM function by TBSS, ALFF and the function–structure coupling images (ALFF divided by FA) were smoothed (6 mm full-width half-maximum, isotropic), and projected onto the skeleton using the non-linear registration and projection vectors from the TBSS analysis for FA images ("*tbss_non_FA*" script in FSL).

2.5 | Functional topology of WM network

By constructing ROI-to-ROI correlation matrix within WM, we estimated the WM network properties in each group, and tested the performance of classifying subjects by functional connectivity patterns.

2.5.1 | Matrix construction

First, an individual WM mask was transformed into MNI space using the matrix from structural normalization. Then, only voxels identified as WM in >90% of subjects were included as part of the group-level WM mask. Second, the group-level WM mask was subdivided into 256 random ROIs with approximately identical size (Fornito, Zalesky, & Bullmore, 2010; Zalesky et al., 2010). This was achieved by half-splitting the target mask (i.e., the whole WM mask and its sub-masks) recursively. In each half-splitting, two seed voxels with the largest distance were identified within the target mask. Then, other voxels were classified into submasks according to their distance to the seed voxels. Third, a correlation matrix was produced by Pearson's correlation analysis between each paired ROI.

2.5.2 | Network properties

Six global topologies were computed here: network strength (S_p), global efficiency (E_{glob}), local efficiency (E_{loc}), shortest path length (L_p), clustering coefficient (C_p), and small worldness (σ). A recent review describes the uses and interpretations of these network measures (Rubinov & Sporns, 2010). These measures were computed using the Brain Connectivity Toolbox (http://www.brain-connectivity-toolbox.net/).

Network strength: For a network graph (G) with a given number of nodes (N), the strength of G was calculated as follows:

$$S_p(G) = \frac{1}{N}\sum_{i \in G} S(i),$$

where $S(i)$ is the sum of edge weights, w_{ij}—which are correlation coefficient values for weighted networks—linking to node i. Network strength is the average strength across all of the nodes in the network.

Small-world properties: Small-world network parameters C_p, and L_p were originally proposed by Watts and Strogatz (1998). The clustering coefficient of a node i [$C(i)$] was defined as the extent to which the neighborhoods were connected with each other or not, and was computed as follows:

$$C(i) = \frac{\sum_{j,h \in N}\left(w_{ij}w_{ih}w_{jh}\right)^{1/3}}{k_i(k_i - 1)},$$

where k_i is the number of nodes connected to node i and w is the weight scaled by the mean of all weights to control each participant's cost at the same level. The C_p of a network is the average clustering coefficient over all nodes, and indicates the extent of the local inter-connectivity or cliquishness in a network.

The path length between any pair of nodes (e.g., i and j) was defined as the sum of edge lengths along this path. The shortest path length, L_{ij}, was defined as the shortest length of the path for nodes i and j; for the network G, the shortest path length (L_p) is the average L_{ij} across all the paired nodes. L_p quantifies the ability for information propagation, with larger L_p indicating lower propagation efficiency.

To examine small world properties related to C_p and L_p, brain networks were compared to random networks. A small world network has similar path length but higher clustering than a random network; that is, $\gamma = C_p^{real}/C_p^{rand} > 1$ and $\lambda = L_p^{real}/L_p^{rand} \approx 1$ (Watts & Strogatz,
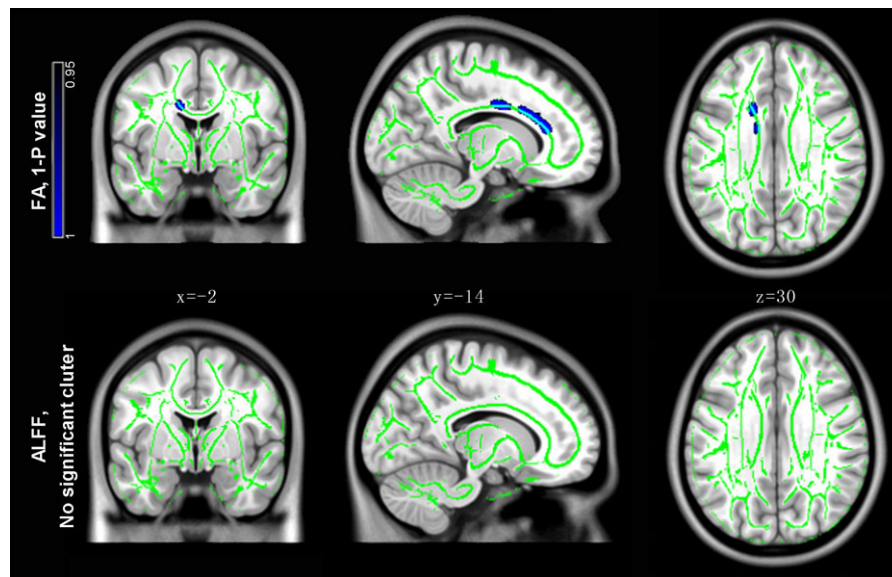
FIGURE 2 Tract-based spatial statistics on fractional anisotropy (FA) and amplitude of low-frequency fluctuation (ALFF). Patients showed significantly decreased FA in the left cingulum as compared to healthy controls. No significant difference was found in ALFF between groups. The fiber skeleton is illustrated in green [Color figure can be viewed at wileyonlinelibrary.com]

1998). These two conditions can be summarized as a scalar quantitative measurement—that is, small-worldness, $\sigma = \gamma/\lambda$—that is, typically >1 in the case of small world organization (Achard, Salvador, Whitcher, Suckling, & Bullmore, 2006; Humphries, Gurney, & Prescott, 2006). For each individual brain network, a set of 100 comparable random networks with similar degree distribution and symmetric adjacent matrices was formed, and C_p^{rand} and L_p^{rand} were defined as the average weighted clustering coefficient and weighted path length.

Network efficiency: The global efficiency of G measures the global efficiency of parallel information transfer in the network (Latora & Marchiori, 2001), which can be computed as follows:

$$E_{\text{glob}}(G) = \frac{1}{N(N-1)} \sum_{i \neq j \in G} \frac{1}{L_{ij}},$$

where L_{ij} is the shortest path length between nodes i and j in G. The local efficiency of G reveals how much the network is fault-tolerant, and demonstrates the efficiency of communication among the first neighbors of node i when it is removed. The local efficiency of a graph is defined as follows:

$$E_{\text{loc}}(G) = \frac{1}{N} \sum_{i \in G} E_{\text{glob}}(G_i),$$

where G_i denotes the subgraph composed of the nearest neighbors of node i.

2.5.3 | Connectome-based classification

This classification was performed based on the ROI-to-ROI correlation matrix (Fisher's r-to-z transformed), and estimated by leave-one-out cross validation. We sequentially selected one subject as a test and estimated its similarity to mean correlation matrices across the rest of the patients and controls by Pearson's correlation. The test subject would be assigned to the group with the higher correlation coefficient. After 109 rounds of classification, the performance could be estimated by sensitivity, specificity, accuracy, and area under the curve

(AUC) of the receiver operating characteristic (ROC). Sensitivity and specificity referred to the percentage of cases that correctly identified as patient and control, respectively. Accuracy referred to the total proportion of samples correctly classified. The ROC curves provided information regarding the balance between sensitivity and the false positive rate (1-specificity) across a range of decision thresholds.

2.6 | Statistical analysis

Randomized script in FSL was used to test for between-group differences in the skeletonized data (i.e., FA, ALFF, and ALFF/FA), with age, gender, and education as covariates. It performed permutation-based testing (5,000 times) and inference using Threshold-Free Cluster Enhancement (TFCE) (Nichols & Holmes, 2002) with a threshold of $P_{\text{corr}} < 0.05$, corrected for multiple comparisons.

Based on the findings of between-group comparisons of ALFF/FA ratios, the significant cluster was defined as seed region, then the average signal within this seed was correlated to each voxel in the ipsilateral corticobasal ganglia-thalamocortical (CBTC) network (Pearson's correlation-based functional connectivity). The left CBTC mask included the left primary motor area, primary somatosensory area, supplementary motor area from an automatic anatomical labeling template (Tzourio-Mazoyer et al., 2002), and subcortical structures from our previous meta-analysis of PD (including the left caudate, putamen, globus pallidus, pedunculopontine nucleus, and subthalamic nucleus) (Ji et al., 2018), see Supporting Information Figure S1. Between-group comparisons were performed by a permutation test through a toolbox in SPM12, Statistic non-Parameter Mapping (SnPM). Briefly, it randomized the label ("patient" or "control") of each subject 5,000 times. In each trial, a two-sample t test would produce a t map. Based on the distribution of these 5,000 t maps, the t value in the real labeling condition can be inferred as significant or not (Nichols & Holmes, 2002). To control the family-wise error in multiple comparisons, we first set a cluster-defined threshold t, 2.37 (corresponding to
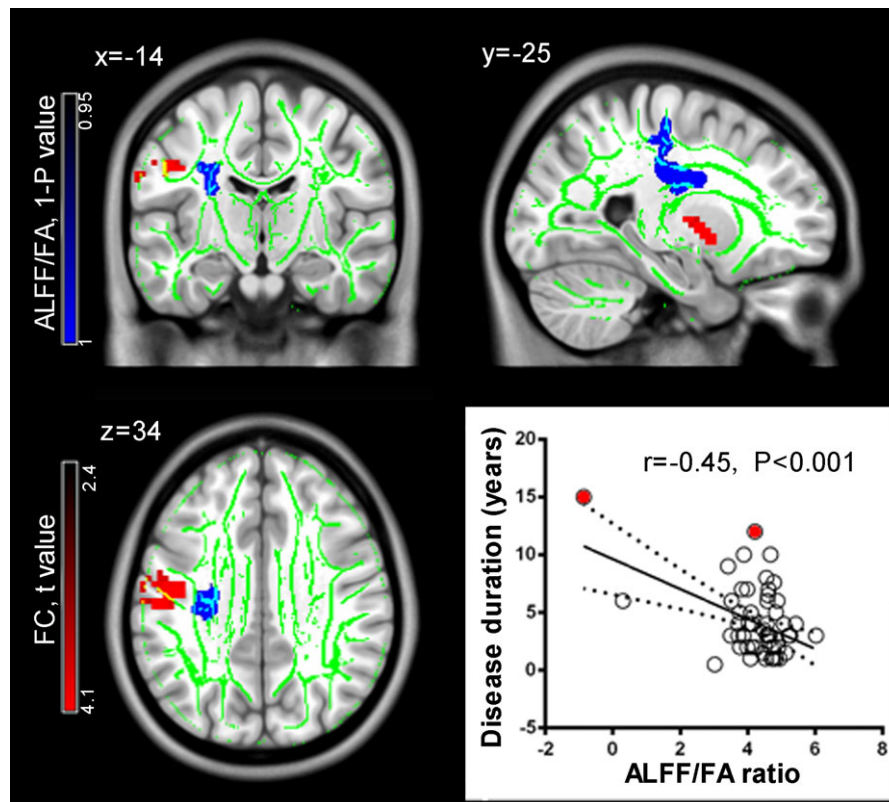
FIGURE 3 Structural and functional alterations in the left corticobasal ganglia-thalamocortical network in Parkinson's disease (PD). PD patients exhibit decreased amplitude of low-frequency fluctuation (ALFF)/fractional anisotropy (FA) ratio in the corticospinal tracts (shown here in blue) and increased white matter (WM)—Gray matter (GM) functional connectivity (shown here in red). The fiber skeleton for tract-based spatial statistics is illustrated in green. In the patient group, the abnormal ALFF/FA ratio in the corticospinal tract shows a significant negative correlation with disease duration. Notably, this correlation become nonsignificant after removing two statistical outliers marked in red color [Color figure can be viewed at wileyonlinelibrary.com]

$p = .01$ at the voxel level). Then, only clusters larger than a given volume would be reported as having survived the cluster-level correction, $P_{corr} < 0.05$.

Pearson correlation analyses were performed between the imaging data and clinical measurements (disease duration, UPDRS-III score, and H-Y stage) in the patients. Notably, the UPDRS-III and H-Y information were only available for 55 and 50 patients, respectively. Potential outliers were identified by nonlinear regression analyses in GraphPad Prism (Motulsky & Brown, 2006).

Permutation tests were used to show the significance of classification measures. Briefly, subjects (except the test subject) were randomly assigned to patient and control group 5,000 times, with insurance that each group had the same number of subjects as the real condition. Based on the distribution of these 5,000 classification measures, the significance of the discriminative performance in the real condition was determined with $p < .05$ as a cut-off for significance.

To compare the WM network property between patients and controls, we controlled differences in edge numbers across subjects by applying a sparsity threshold to all correlation matrices. Sparsity was defined as the ratio of the number of existing edges divided by the maximum possible number of edges in a network. This approach normalized the number of edges for all resultant networks by applying a subject-specific correlation coefficient threshold, and minimized the

effects of possible discrepancies in the overall correlation strength between groups (Wig, Schlaggar, & Petersen, 2011). Instead of selecting a single threshold, we repeatedly determined a threshold for each correlation matrix over a wide range of sparsity levels according to the following criteria: the lower range of sparsity was defined as the average degree of a node (i.e., the number of connections linked to the node) over all nodes of each thresholded network, which was $>2 \times \log(N)$, with N = 256 denoting the number of nodes. The upper range of sparsity corresponded to the lowest significant correlation coefficient ($p < .05$) among all subjects. This generated the range of thresholds of $0.04 \leq S \leq 0.40$. Finally, the area under the global property curve was evaluated by a two-sample t test, which provided an overall estimation independent of the sparsity threshold.

2.7 | Supplementary analysis

To estimate the influence of medication, global signal regression, and head motion, on our findings, we performed additional analyses. (1) We excluded the six patients in a medication-on stage and repeated all the analyses. (2) We regressed out the average global signal during functional data processing and kept all other processes. (3) We did not delete functional data according to head motion parameters in the primary report, since this process is still in debate. Its influence on our findings was estimated here. We assessed framewise displacement (FD) for each functional volume (Power, Barnes,

(a)   Matrix construction

White matter ROIs

Time series

Correlation matrix
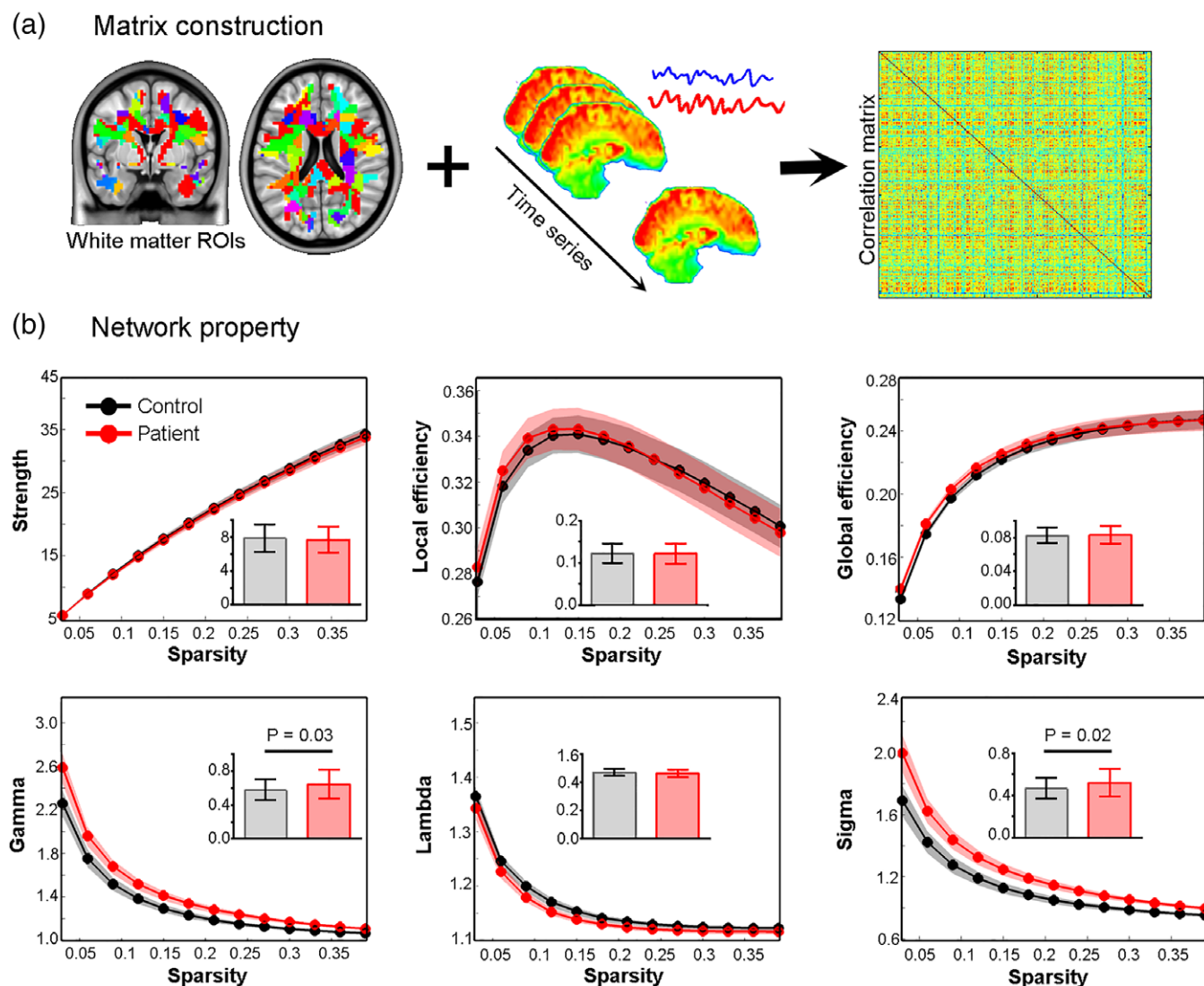
(b)   Network property

FIGURE 4   Network construction and property comparison. White matter network was constructed by correlation analysis between 256 random region-of-interests (a). Curves displaying the quantification of global topologies of functional networks in patient and control groups (b). Inset maps (with mean and *SD*) show significant between-group differences in the area under the curve in network efficiency (gamma), and small-worldness (sigma). Colored shadows indicate the *SD* of global properties across sparsities [Color figure can be viewed at wileyonlinelibrary.com]

Snyder, Schlaggar, & Petersen, 2012). Along with the bad time points (FD > 0.5 mm), one preceding and two following points were deleted as an additional preprocessing step prior to computing imaging measures (i.e., ALFF and functional connectivity).

3 | RESULTS

3.1 | Demographic characteristics

No significant differences were found in age, male/female ratio, years of education, and cognitive scores between PD and controls (Table 1). The FD (Power et al., 2012) was also similar between groups ($t = 0.25$, $p = .80$).

3.2 | WM structural-functional coupling

TBSS analysis indicated significant between-group differences in FA and ALFF/FA, but not ALFF ($P_{corr} < 0.05$). Significantly decreased FA

and ALFF/FA was found in the left cingulum and left corticospinal tract, respectively, in PD patients relative to controls (Figure 2 and 3). See the smoothing kernel effect on ALFF/FA comparison in Supporting Information Figure S2. Pearson's correlation analysis indicated that the ALFF/FA ratio of the left-corticospinal cluster negatively correlated with disease duration ($r = -0.45$, $p = .0005$, Figure 3), but not H-Y ($r = -0.09$, $p = .51$) or UPDRS-III ($r = -0.05$, $p = .74$) scores. No significant correlation was found between FA in the left cingulum and clinical measures (all $p > .05$, see statistics in Supporting Information Table S2).

3.3 | WM-GM functional connectivity

Significant cluster in the ALFF/FA analysis was defined as a seed region for this functional connectivity analysis. PD patients showed increased functional connectivity in the left post/precentral gyrus, and left putamen (Figure 3, Supporting Information Table S1, $P_{corr} < 0.05$ in cluster level [voxel-level $p < .01$, cluster size>38 voxels, permutation test]). No significant correlation was found between these

functional abnormalities and the clinical measures in the PD group (all $p > .05$, see statistics in Supporting Information Table S2).

3.4 | WM functional network properties

PD patients showed significantly increased relative C_p (gamma, $t = 2.27$, $p = .03$) and small-world property (sigma, $t = 2.50$, $p = .02$) compared to controls. Other properties (S_p [$t = -0.25$, $p = .81$], E_{local} [$t = -0.06$, $p = .95$], E_{global} [$t = 0.40$, $p = .69$], and lambda [$t = -1.38$, $p = .17$]) were similar between groups (Figure 4). No significant correlation was found between network properties (gamma and sigma) and clinical measures in the PD group (all $p > .05$, see statistics in Supporting Information Table S2). These findings were well-replicated when the WM mask was divided into 128 and 512 random ROIs (Supporting Information Table S3).

3.5 | WM connectome-based classification

Based on the functional connectivity pattern within WM, leave-one-out cross validation indicated that PD patients could be discriminated from healthy controls with 73% accuracy (75% sensitivity, 70% specificity), and 75% AUC (both permutation tests were significant at $p < .005$).

3.6 | Complementary analysis

Among the four types of measurements (ALFF/FA ratio, WM-GM functional connectivity, network property, and connectome-based classification), only the network property findings were not replicated in the "global regression" condition, while the others were reproduced in all the three complementary analyses (Supporting Information Table S4).

4 | DISCUSSION

This study systematically investigated WM function in PD using multi-model MRI data sets. At the regional level, the TBSS analysis indicated a decreased ALFF/FA ratio in the left corticospinal tracts in PD patients, which was aggravated with disease duration. This left corticospinal cluster also showed abnormally increased functional connectivity within the CBTC network in PD patients. At a global level, graph-theoretical analysis indicated abnormally increased C_p and small-world properties in PD patients. Furthermore, the WM functional connectome showed fair performance (73% accuracy and 75% AUC) in discriminating PD patients from controls. In summary, our findings characterized the regional and network functioning of WM in PD, providing important information for the understanding of PD pathophysiology.

Changes in brain structure and function have been extensively investigated with neuroimaging studies in order to reveal the pathophysiology of PD (Ji et al., 2018; Li, Ren, Cao, & Huang, 2018). Although many TBSS studies have investigated WM in PD, the number of patients analyzed was less than 30 in most studies (Ji, Wang, Zhu, Liu, & Shi, 2015; Li et al., 2018; Worker et al., 2014). This limitation may increase sample heterogeneity between studies, resulting in

quite different findings that may be difficult to replicate. For instance, while some studies reported no significant FA abnormality in PD patients (Hattori et al., 2012; Worker et al., 2014), others found widespread FA changes (Li et al., 2018). Using a large sample-size (170 patients), Galantucci and colleagues found significant FA decreases in the corpus collosum and associative frontoparietal tracts in PD patients relative to controls (Galantucci et al., 2017). Consistent with this, we found significantly decreased FA in the left cingulum connecting the frontal and parietal cortices.

In addition to the conventional measure (i.e., FA), two novel measures (i.e., ALFF and ALFF/FA) were adopted for investigating WM function and structural-functional coupling. In PD patients, abnormality was only found in the ALFF/FA but not ALFF. FA and ALFF were complementary measures reflecting WM structure and function, and showed significant correlation in healthy subjects (Ji, Liao, et al., 2017). In pathological condition, this structural-functional coupling may be disrupted and the three measures showed different changes in patients. Similarly, functional connectivity strength (FCS) and cerebral blood flow (CBF) showed significant correlation in healthy subjects (Liang, Zou, He, & Yang, 2013), but their abnormalities were distinct to FCS/CBF ratio in schizophrenia patients (Zhu et al., 2017). In this study, we found the left corticospinal tracts showing abnormally low ALFF/FA in PD patients, which is consistent with the core PD symptom observed in the clinic (i.e., impaired motor function). This result suggests that structural-functional coupling is a sensitive WM measure to detect the neuropathological changes in PD. Furthermore, as the left corticospinal tracts showed abnormal connectivity with cortical and subcortical nodes within motor network in PD patients, our findings indicate that this WM substruction does not properly functionally connect cortical (post/precentral gyrus) and subcortical (putamen) nodes. Further studies are needed to investigate whether the increased WM-GM functional connectivity is a compensatory change in the PD brain. Taken together, the FA, ALFF, and ALFF/FA ratio could provide complementary information and should be jointly used to reveal pathological changes in schizophrenia.

Graph theory provides a network perspective for investigating how different regions of the brain work interactively. In both healthy and disease conditions, the WM structural and GM functional features have been extensively investigated by graph-theoretical analysis on diffusion and fMRI data, respectively (Gong et al., 2009; Ji et al., 2016; Ji, Zhang, et al., 2015). It has been demonstrated that the human brain is organized in a "small-world" pattern to produce high value for low energetic cost (Bullmore & Sporns, 2012). In this study, we investigated the functional architecture of the WM network using resting-state fMRI. Both healthy controls and PD patients showed a small-world property (gamma > 1, and lambda $\cong$ 1), but the patients indicated greater gamma and sigma. Gamma is the global clustering coefficient of a real network relative to a random network. The increase in sigma (the ratio of gamma and lambda) observed in patients was mainly a result of an alteration in gamma, as the lambda was similar between groups. This pattern of WM functional reconfiguration can be summarized as a shift to higher integrative capacity with low additional expense of metabolic connection costs. Conversely, WM functional networks become more optimal in PD patients. This was different from previous findings concerning WM

structure (Galantucci et al., 2017) and GM function (Gottlich et al., 2013; Kim et al., 2017) in PD patients, and suggests a functional-structural decoupling at the network level.

Our findings also have several clinical implications. First, we hypothesized that a group of subjects with common behavior possess a similar functional WM connectome (Finn et al., 2015; Miranda-Dominguez et al., 2014), and that subjects could therefore be classified according to their connectome similarity with candidate groups. The classification indicated fair performance with 73% accuracy, and 75% AUC. To improve their performance, future studies should adopt an individualized functional atlas rather than group parcellation for cross-subject alignment (Wang et al., 2015), and a movement-related rather than resting-state design (Finn et al., 2017). Second, transcranial magnetic stimulation (TMS) is an noninvasive neuro-modulation technique, which has shown potential to treat PD (Chou, Hickey, Sundman, Song, & Chen, 2015); however, its mechanism is still largely unknown. In addition, most TMS equipment can only effectively stimulate superficial cortical areas. It has been hypothesized that the after-effects of stimulation could reach distant areas via structural connections, but how fiber tracts are functionally modulated by TMS and interact with cortical and subcoritcal nuclei remains to be determined. Our findings suggest that the ALFF/FA ratio may be used as a potential biomarker to understand the mechanism of TMS in PD treatment.

There were some limitations in this study. First, to exclude any short-term effect of medication on the results, most patients were evaluated in a medication-off state. However, the long-term effect of medication still presumably persisted in these patients. Future studies with drug-naïve patients are necessary to address this issue. Second, unlike in GM, the physiological basis of the BOLD signal in WM is still undetermined. In a systematic review, Gawryluk and colleagues suggested that the hemodynamic changes in WM may relate to the energetic requirement for spiking activity, maintenance of resting potential and neuronal housekeeping processes, whereas the contribution of artifacts (such as motion, partial volume, and physiological noise) was minimal (Gawryluk, Mazerolle, & D'Arcy, 2014). In this study, the possible effect of artifacts was also accounted for by regression of motion parameters, regression of CSF signal, and independent processing for GM and WM. Future neurophysiological studies on the WM BOLD signal are imperative to further explain the current findings in PD patients. Third, in accordance with previous studies (Ji, Liao, et al., 2017; Jiang et al., 2018; Peer et al., 2017), our main findings were based on data without global signal regression, but the complementary analysis indicated the findings of WM network properties may be sensitive to this processing. The effect of global signal regression has long been discussed when estimating GM function (Murphy & Fox, 2016); yet more specific investigations are needed to show its influence on WM functional analysis.

5 | CONCLUSION

This study investigated WM function in PD using resting-state fMRI. At the regional level, the left corticospinal tract in PD patients showed decreased functional-structural coupling and increased synchronization with the CBTC nodes. At the global level, the WM functional network in patients showed small-world properties and was abnormally increased, compared to healthy controls. In summary, these findings on WM function provide a complement to conventional structural studies, which together are important for understanding the pathophysiology of PD.

ORCID

Gong-Jun Ji 🔟 https://orcid.org/0000-0002-7073-5534

REFERENCES

Aarabi, M. H., Kamalian, A., Mohajer, B., Shandiz, M. S., Eqlimi, E., Shojaei, A., & Safabakhsh, H. (2015). A statistical approach in human brain connectome of Parkinson disease in elderly people using network based statistics. *Conference Proceedings: Annual International Conference of the IEEE Engineering in Medicine and Biology Society*, *2015*, 4310–4313.

Achard, S., Salvador, R., Whitcher, B., Suckling, J., & Bullmore, E. (2006). A resilient, low-frequency, small-world human brain functional network with highly connected association cortical hubs. *The Journal of Neuroscience*, *26*, 63–72.

Ashburner, J. (2007). A fast diffeomorphic image registration algorithm. *NeuroImage*, *38*, 95–113.

Atkinson-Clement, C., Pinto, S., Eusebio, A., & Coulon, O. (2017). Diffusion tensor imaging in Parkinson's disease: Review and meta-analysis. *Neuroimage: Clinical*, *16*, 98–110.

Bullmore, E., & Sporns, O. (2009). Complex brain networks: Graph theoretical analysis of structural and functional systems. *Nature Reviews. Neuroscience*, *10*, 186–198.

Bullmore, E., & Sporns, O. (2012). The economy of brain network organization. *Nature Reviews. Neuroscience*, *13*, 336–349.

Burke, R. E., & O'Malley, K. (2013). Axon degeneration in Parkinson's disease. *Experimental Neurology*, *246*, 72–83.

Chen, X., Zhang, H., Zhang, L., Shen, C., Lee, S. W., & Shen, D. (2017). Extraction of dynamic functional connectivity from brain grey matter and white matter for MCI classification. *Human Brain Mapping*, *38*, 5019–5034.

Chou, Y. H., Hickey, P. T., Sundman, M., Song, A. W., & Chen, N. K. (2015). Effects of repetitive transcranial magnetic stimulation on motor symptoms in Parkinson disease: A systematic review and meta-analysis. *JAMA Neurology*, *72*, 432–440.

Cochrane, C. J., & Ebmeier, K. P. (2013). Diffusion tensor imaging in parkinsonian syndromes: A systematic review and meta-analysis. *Neurology*, *80*, 857–864.

Courtemanche, M. J., Sparrey, C. J., Song, X., MacKay, A., & D'Arcy, R. C. N. (2018). Detecting white matter activity using conventional 3 tesla fMRI: An evaluation of standard field strength and hemodynamic response function. *NeuroImage*, *169*, 145–150.

Desikan, R. S., Segonne, F., Fischl, B., Quinn, B. T., Dickerson, B. C., Blacker, D., … Killiany, R. J. (2006). An automated labeling system for subdividing the human cerebral cortex on MRI scans into gyral based regions of interest. *NeuroImage*, *31*, 968–980.

Ding, Z., Huang, Y., Bailey, S. K., Gao, Y., Cutting, L. E., Rogers, B. P., … Gore, J. C. (2018). Detection of synchronous brain activity in white matter tracts at rest and under functional loading. *Proceedings of the National Academy of Sciences of the United States of America*, *115*, 595–600.

Ding, Z., Newton, A. T., Xu, R., Anderson, A. W., Morgan, V. L., & Gore, J. C. (2013). Spatio-temporal correlation tensors reveal functional structure in human brain. *PLoS One*, *8*, e82107.

Dorsey, E. R., Constantinescu, R., Thompson, J. P., Biglan, K. M., Holloway, R. G., Kieburtz, K., … Tanner, C. M. (2007). Projected number of people with Parkinson disease in the most populous nations, 2005 through 2030. *Neurology*, *68*, 384–386.

Fabri, M., Pierpaoli, C., Barbaresi, P., & Polonara, G. (2014). Functional topography of the corpus callosum investigated by DTI and fMRI. *World Journal of Radiology*, *6*, 895–906.

Fabri, M., & Polonara, G. (2013). Functional topography of human corpus callosum: An FMRI mapping study. *Neural Plasticity*, *2013*, 251308.

Fabri, M., Polonara, G., Mascioli, G., Salvolini, U., & Manzoni, T. (2011). Topographical organization of human corpus callosum: An fMRI mapping study. *Brain Research*, *1370*, 99–111.

Finn, E. S., Scheinost, D., Finn, D. M., Shen, X., Papademetris, X., & Constable, R. T. (2017). Can brain state be manipulated to emphasize individual differences in functional connectivity. *NeuroImage*, *160*, 140–151.

Finn, E. S., Shen, X., Scheinost, D., Rosenberg, M. D., Huang, J., Chun, M. M., … Constable, R. T. (2015). Functional connectome fingerprinting: Identifying individuals using patterns of brain connectivity. *Nature Neuroscience*, *18*, 1664–1671.

Fornito, A., Zalesky, A., & Bullmore, E. T. (2010). Network scaling effects in graph analytic studies of human resting-state FMRI data. *Frontiers in Systems Neuroscience*, *4*, 22.

Friston, K. J., Williams, S., Howard, R., Frackowiak, R. S., & Turner, R. (1996). Movement-related effects in fMRI time-series. *Magnetic Resonance in Medicine*, *35*, 346–355.

Galantucci, S., Agosta, F., Stefanova, E., Basaia, S., van den Heuvel, M. P., Stojkovic, T., … Filippi, M. (2017). Structural brain Connectome and cognitive impairment in Parkinson disease. *Radiology*, *283*, 515–525.

Gawryluk, J. R., D'Arcy, R. C., Mazerolle, E. L., Brewer, K. D., & Beyea, S. D. (2011). Functional mapping in the corpus callosum: A 4T fMRI study of white matter. *NeuroImage*, *54*, 10–15.

Gawryluk, J. R., Mazerolle, E. L., Beyea, S. D., & D'Arcy, R. C. (2014). Functional MRI activation in white matter during the symbol digit modalities test. *Frontiers in Human Neuroscience*, *8*, 589.

Gawryluk, J. R., Mazerolle, E. L., & D'Arcy, R. C. (2014). Does functional MRI detect activation in white matter? A review of emerging evidence, issues, and future directions. *Frontiers in Neuroscience*, *8*, 239.

Gong, G., He, Y., Concha, L., Lebel, C., Gross, D. W., Evans, A. C., & Beaulieu, C. (2009). Mapping anatomical connectivity patterns of human cerebral cortex using in vivo diffusion tensor imaging tractography. *Cerebral Cortex*, *19*, 524–536.

Gottlich, M., Munte, T. F., Heldmann, M., Kasten, M., Hagenah, J., & Kramer, U. M. (2013). Altered resting state brain networks in Parkinson's disease. *PLoS One*, *8*, e77336.

Haberling, I. S., Badzakova-Trajkov, G., & Corballis, M. C. (2011). Callosal tracts and patterns of hemispheric dominance: A combined fMRI and DTI study. *NeuroImage*, *54*, 779–786.

Hagmann, P., Cammoun, L., Gigandet, X., Meuli, R., Honey, C. J., Wedeen, V. J., & Sporns, O. (2008). Mapping the structural core of human cerebral cortex. *PLoS Biology*, *6*, e159.

Hall, J. M., Ehgoetz Martens, K. A., Walton, C. C., O'Callaghan, C., Keller, P. E., Lewis, S. J., & Moustafa, A. A. (2016). Diffusion alterations associated with Parkinson's disease symptomatology: A review of the literature. *Parkinsonism & Related Disorders*, *33*, 12–26.

Hattori, T., Orimo, S., Aoki, S., Ito, K., Abe, O., Amano, A., … Mizusawa, H. (2012). Cognitive status correlates with white matter alteration in Parkinson's disease. *Human Brain Mapping*, *33*, 727–739.

Honey, C. J., Sporns, O., Cammoun, L., Gigandet, X., Thiran, J. P., Meuli, R., & Hagmann, P. (2009). Predicting human resting-state functional connectivity from structural connectivity. *Proceedings of the National Academy of Sciences of the United States of America*, *106*, 2035–2040.

Humphries, M. D., Gurney, K., & Prescott, T. J. (2006). The brainstem reticular formation is a small-world, not scale-free, network. *Proceedings of the Biological Sciences*, *273*, 503–511.

Ji, G. J., Hu, P., Liu, T. T., Li, Y., Chen, X., Zhu, C., … Wang, K. (2018). Functional connectivity of the Corticobasal ganglia-Thalamocortical network in Parkinson disease: A systematic review and meta-analysis with cross-validation. *Radiology*, *287*, 973–982.

Ji, G. J., Liao, W., Chen, F. F., Zhang, L., & Wang, K. (2017). Low-frequency blood oxygen level-dependent fluctuations in the brain white matter: More than just noise. *Science Bulletin*, *62*, 656–657.

Ji, G. J., Yu, F., Liao, W., & Wang, K. (2017). Dynamic aftereffects in supplementary motor network following inhibitory transcranial magnetic stimulation protocols. *NeuroImage*, *149*, 285–294.

Ji, G. J., Yu, Y., Miao, H. H., Wang, Z. J., Tang, Y. L., & Liao, W. (2016). Decreased network efficiency in benign epilepsy with Centrotemporal spikes. *Radiology*, *283*, 186–194.

Ji, G. J., Zhang, Z., Xu, Q., Wei, W., Wang, J., Wang, Z., … Lu, G. (2015). Connectome reorganization associated with surgical outcome in temporal lobe epilepsy. *Medicine (Baltimore)*, *94*, e1737.

Ji, L., Wang, Y., Zhu, D., Liu, W., & Shi, J. (2015). White matter differences between multiple system atrophy (parkinsonian type) and Parkinson's disease: A diffusion tensor image study. *Neuroscience*, *305*, 109–116.

Jiang, Y., Luo, C., Li, X., Li, Y., Yang, H., Li, J., … Yao, D. (2018). White-matter functional networks changes in patients with schizophrenia. *NeuroImage*, https://doi.org/10.1016/j.neuroimage.2018.04.018.

Kim, J., Criaud, M., Cho, S. S., Diez-Cirarda, M., Mihaescu, A., Coakeley, S., … Strafella, A. P. (2017). Abnormal intrinsic brain functional network dynamics in Parkinson's disease. *Brain*, *140*, 2955–2967.

Latora, V., & Marchiori, M. (2001). Efficient behavior of small-world networks. *Physical Review Letters*, *87*, 198701.

Li, C., Huang, B., Zhang, R., Ma, Q., Yang, W., Wang, L., … Huang, R. (2017). Impaired topological architecture of brain structural networks in idiopathic Parkinson's disease: A DTI study. *Brain Imaging and Behavior*, *11*, 113–128.

Li, X. R., Ren, Y. D., Cao, B., & Huang, X. L. (2017). Analysis of white matter characteristics with tract-based spatial statistics according to diffusion tensor imaging in early Parkinson's disease. *Neuroscience Letters*, *675*, 127–132.

Li, X. R., Ren, Y. D., Cao, B., & Huang, X. L. (2018). Analysis of white matter characteristics with tract-based spatial statistics according to diffusion tensor imaging in early Parkinson's disease. *Neuroscience Letters*, *675*, 127–132.

Liang, X., Zou, Q., He, Y., & Yang, Y. (2013). Coupling of functional connectivity and regional cerebral blood flow reveals a physiological basis for network hubs of the human brain. *Proceedings of the National Academy of Sciences of the United States of America*, *110*, 1929–1934.

Makedonov, I., Chen, J. J., Masellis, M., & MacIntosh, B. J. (2016). Physiological fluctuations in white matter are increased in Alzheimer's disease and correlate with neuroimaging and cognitive biomarkers. *Neurobiology of Aging*, *37*, 12–18.

Marussich, L., Lu, K. H., Wen, H., & Liu, Z. (2017). Mapping white-matter functional organization at rest and during naturalistic visual perception. *NeuroImage*, *146*, 1128–1141.

Mazerolle, E. L., Beyea, S. D., Gawryluk, J. R., Brewer, K. D., Bowen, C. V., & D'Arcy, R. C. (2010). Confirming white matter fMRI activation in the corpus callosum: Co-localization with DTI tractography. *NeuroImage*, *50*, 616–621.

Mazerolle, E. L., D'Arcy, R. C., & Beyea, S. D. (2008). Detecting functional magnetic resonance imaging activation in white matter: Interhemispheric transfer across the corpus callosum. *BMC Neuroscience*, *9*, 84.

Miranda-Dominguez, O., Mills, B. D., Carpenter, S. D., Grant, K. A., Kroenke, C. D., Nigg, J. T., & Fair, D. A. (2014). Connectotyping: Model based fingerprinting of the functional connectome. *PLoS One*, *9*, e111048.

Motulsky, H. J., & Brown, R. E. (2006). Detecting outliers when fitting data with nonlinear regression - a new method based on robust nonlinear regression and the false discovery rate. *BMC Bioinformatics*, *7*, 123.

Murphy, K., & Fox, M. D. (2016). Towards a consensus regarding global signal regression for resting state functional connectivity MRI. *NeuroImage*, *154*, 169–173.

Nichols, T. E., & Holmes, A. P. (2002). Nonparametric permutation tests for functional neuroimaging: A primer with examples. *Human Brain Mapping*, *15*, 1–25.

Nigro, S., Riccelli, R., Passamonti, L., Arabia, G., Morelli, M., Nistico, R., ... Quattrone, A. (2016). Characterizing structural neural networks in de novo Parkinson disease patients using diffusion tensor imaging. *Human Brain Mapping*, *37*, 4500–4510.

Peer, M., Nitzan, M., Bick, A. S., Levin, N., & Arzy, S. (2017). Evidence for functional networks within the human Brain's white matter. *The Journal of Neuroscience*, *37*, 6394–6407.

Pereira, J. B., Aarsland, D., Ginestet, C. E., Lebedev, A. V., Wahlund, L. O., Simmons, A., ... Westman, E. (2015). Aberrant cerebral network topology and mild cognitive impairment in early Parkinson's disease. *Human Brain Mapping*, *36*, 2980–2995.

Power, J. D., Barnes, K. A., Snyder, A. Z., Schlaggar, B. L., & Petersen, S. E. (2012). Spurious but systematic correlations in functional connectivity MRI networks arise from subject motion. *NeuroImage*, *59*, 2142–2154.

Rubinov, M., & Sporns, O. (2010). Complex network measures of brain connectivity: Uses and interpretations. *NeuroImage*, *52*, 1059–1069.

Schwarz, S. T., Abaei, M., Gontu, V., Morgan, P. S., Bajaj, N., & Auer, D. P. (2013). Diffusion tensor imaging of nigral degeneration in Parkinson's disease: A region-of-interest and voxel-based study at 3 T and systematic review with meta-analysis. *Neuroimage: Clinical*, *3*, 481–488.

Smith, S. M., Jenkinson, M., Johansen-Berg, H., Rueckert, D., Nichols, T. E., Mackay, C. E., ... Behrens, T. E. (2006). Tract-based spatial statistics: Voxelwise analysis of multi-subject diffusion data. *NeuroImage*, *31*, 1487–1505.

Tagliaferro, P., Kareva, T., Oo, T. F., Yarygina, O., Kholodilov, N., & Burke, R. E. (2015). An early axonopathy in a hLRRK2(R1441G) transgenic model of Parkinson disease. *Neurobiology of Disease*, *82*, 359–371.

Tzourio-Mazoyer, N., Landeau, B., Papathanassiou, D., Crivello, F., Etard, O., Delcroix, N., ... Joliot, M. (2002). Automated anatomical labeling of activations in SPM using a macroscopic anatomical parcellation of the MNI MRI single-subject brain. *NeuroImage*, *15*, 273–289.

Wang, D., Buckner, R. L., Fox, M. D., Holt, D. J., Holmes, A. J., Stoecklein, S., ... Liu, H. (2015). Parcellating cortical functional networks in individuals. *Nature Neuroscience*, *18*, 1853–1860.

Wang, Z., Dai, Z., Gong, G., Zhou, C., & He, Y. (2014). Understanding structural-functional relationships in the human brain: A large-scale network perspective. *The Neuroscientist*, *21*, 290–305.

Watts, D. J., & Strogatz, S. H. (1998). Collective dynamics of 'small-world' networks. *Nature*, *393*, 440–442.

Wig, G. S., Schlaggar, B. L., & Petersen, S. E. (2011). Concepts and principles in the analysis of brain networks. *Annals of the New York Academy of Sciences*, *1224*, 126–146.

Worker, A., Blain, C., Jarosz, J., Chaudhuri, K. R., Barker, G. J., Williams, S. C., ... Simmons, A. (2014). Diffusion tensor imaging of Parkinson's disease, multiple system atrophy and progressive supranuclear palsy: A tract-based spatial statistics study. *PLoS One*, *9*, e112638.

Wu, X., Yang, Z., Bailey, S. K., Zhou, J., Cutting, L. E., Gore, J. C., & Ding, Z. (2017). Functional connectivity and activity of white matter in somatosensory pathways under tactile stimulations. *NeuroImage*, *152*, 371–380.

Yan, C.-G., & Zang, Y.-F. (2010). DPARSF: A MATLAB toolbox for "pipeline" data analysis of resting-state fMRI. *Frontiers in Systems Neuroscience*, *4*, 13.

Zalesky, A., Fornito, A., Harding, I. H., Cocchi, L., Yucel, M., Pantelis, C., & Bullmore, E. T. (2010). Whole-brain anatomical networks: Does the choice of nodes matter. *NeuroImage*, *50*, 970–983.

Zhu, J., Zhuo, C., Xu, L., Liu, F., Qin, W., & Yu, C. (2017). Altered coupling between resting-state cerebral blood flow and functional connectivity in schizophrenia. *Schizophrenia Bulletin*, *43*, 1363–1374.

SUPPORTING INFORMATION

Additional supporting information may be found online in the Supporting Information section at the end of the article.